Supporting Information

Stabilizing O3-Type Layered Oxide Cathodes via Dual-Site Co-Doping for Long-Life Sodium-Ion Batteries

Xuejie Bai,[a] Qian Yang,[a] Yaning Wu,[a] Mingyue Li,[a] Genliang Yu,[a] Tongtong Huo,[a] Xiaobo Zhang,[a] Jie Xu,[a] Xunzhu Zhou,[b] Ting Lv,[a] Lin Li,*[b] Kaixiang Lei,*[a] and Shijian Zheng,*[a]

[a] X. Bai, Q. Yang, Y. Wu, M. Li, G. Yu, T. Huo, X. Zhang, J. Xu, T. Lv, Dr. K. Lei, Prof. S. Zheng
Tianjin Key Laboratory of Materials Laminating Fabrication and Interface Control Technology, School of Materials Science and Engineering, Hebei University of Technology Tianjin 300401, China
E-mail: kaixianglei@hebut.edu.cn, sjzheng@hebut.edu.cn

[b] Dr. X. Zhou, Prof. L. Li
College of Chemistry and Materials Engineering, Wenzhou University Wenzhou, Zhejiang 325035, China
E-mail: linli@wzu.edu.cn

Experimental Section

Materials and Chemicals: The $Na_{0.98}Ca_{0.01}Ni_{0.33}Fe_{0.28}Ti_{0.05}Mn_{0.315}Sn_{0.015}O_2$ (CST-NFM) was achieved through a simple solid-phase reaction. Specifically, reagents such as Na_2CO_3 (excess 5%, Aladdin, 99.80%), $CaCO_3$ (Aladdin, 99.99%), NiO (Aladdin, 99.00%), Fe_2O_3 (Aladdin, 99.00%), MnO_2 (Aladdin, 99.00%), TiO_2 (Aladdin, 99.80%), and SnO_2 (Aladdin, 99.95%) were mixed in a stoichiometric ratio and dispersed in 3mL of anhydrous ethanol to form a homogeneous mixture. This mixture was then placed in a ball mill jar and ball-milled at 900 rpm for 12 hours using agate balls, with a ball-to-material mass ratio of 6:1. Subsequently, the obtained powder mixture was transferred to a constant temperature oven and dried at 80℃ for 1h. Subsequently, the dried powder was ground, and 1g of the ground sample was weighed and placed in a muffle furnace for annealing under air atmosphere. The thermal treatment was carried out as follows: heating to 450°C at a rate of 5°C/min for calcination and holding for 5hours, then continuing to raise the temperature to 900°C and maintaining for 15hours. After completion, the sample was promptly transferred into an argon-filled glove box for storage and further use. The synthesis method for the NFM material is similar, with the only difference being the stoichiometric ratios.

Materials Characterization: The crystalline phase of the synthesized samples was examined via powder X-ray diffraction (XRD) on a Rigaku SmartLab 9kW diffractometer with Cu Kα radiation (λ=1.54 Å) across a 2θ range from 10° to 80°, employing a scan rate of $6°min^{-1}$ and a step size of 0.02°. They were refined by a GSAS

software. A schematic structure of the sample was obtained by VESTA software. In situ X-ray diffraction tests were conducted in a specially designed cell, with charge-discharge cycles at a current density of 30mA g^{-1} within a voltage range of 2.0-4.2 V, collecting data every 15minutes. The morphology of these samples was captured by Scanning Electron Microscopy (SEM, JEOL JSM7610F). High-Resolution Transmission Electron Microscopy (HRTEM) images, Selected Area Electron Diffraction (SAED) patterns, and Energy-Dispersive Spectroscopy (EDS) spectra were obtained on a JEM-2100F. HAADF-STEM images were obtained on a JEM-ARM200F with an accelerating voltage of 200 kV, and equipped with a cold file emission gun and a double hexapole Cs corrector (CEOS GmbH, Heidelberg, Germany). The metal ratios were determined by inductively coupled plasma-optical emission spectrometry (ICP-OES). The surface composition was investigated by X-ray photoelectron spectroscopy (XPS, Thermo Scientific ESCALAB 250Xi). The X-ray absorption spectra were recorded with a laboratory instrument (easy XAFS 300+). Differential electrochemical mass spectrometry (DEMS) (QMG200, Shanghai Linglu) was used to investigate gas evolution during charging. Electron paramagnetic resonance (EPR) spectra were recorded on a Bruker EMXplus-6/1 spectrometer.

Electrochemical Measurement: CR2032-type coin cells were assembled in an Ar-filled glove box with a Button Cell Sealing Machine (MSK-160E). Among others, sodium disk (12 mm in diameter) was obtained from a fresh Na metal block after rolling and cutting. The cathode material, Super-P, and PVdF were mixed in a weight ratio of 8:1:1 and coated onto aluminum foil with a thickness of 100 micrometers. The coated

foil was then dried under vacuum at 80°C for 12 hours, followed by cutting into cathode electrodes with a diameter of 12 mm. In the half-cell configuration, metallic sodium served as the anode and glass fiber filter paper was employed as the separator. The HC anode underwent 30 pre-cycling cycles in a half-cell before being paired with the CST-NFM cathode to assemble a full cell. The electrolyte consisted of 1.0 M sodium hexafluorophosphate ($NaPF_6$) dissolved in a mixture of ethyl methyl carbonate and propylene carbonate (1:1 by volume), with 2 wt.% fluoroethylene carbonates (FEC) added as an additive. Electrochemical long-term cycling tests at constant and varying rates were carried out on the LAND Battery Test System. Coin cells were evaluated over a voltage range of 2.0-4.2 V for long-term cycling at 1.0 C (150 mA g^{-1}). The rate performance of the cells was tested in steps of 0.1C, 0.2C,0.5C, 1C, 2C, 5C, 10C and 0.1C. The cycling curves (CV) and electrochemical impedance spectroscopy (EIS) of the different electrolytes were measured on a ChenHua electrochemical workstation (CHI660E, CH Instruments Inc.). CV tests were measured on ChenHua electrochemical workstation, the curves were tested at a scanning rate of 0.1mV s^{-1} for different cycle numbers in the voltage range of 2.0-4.2 V. The electrochemical CV curves were also evaluated at different scan rate of 0.1, 0.2, 0.4, 0.6, 0.8, and 1.0mV s^{-1}. EIS was performed in a scanning frequency range from 10^5 Hz to 10^{-1} Hz at open circuit potential with an amplitude of 5.0mV.

The diffusion coefficient of Na in the cathode was measured through the galvanostatic intermittent titration technique (GITT) before and after cycling by repeatedly applying 0.1 C current for 10 min and resting for 120 min. D_{Na+} results were

calculated using the equation in the following:

$$D = \frac{4}{\pi\tau}\left(\frac{m_B V_M}{M_B S}\right)^2\left(\frac{\Delta E_S}{\Delta E_\tau}\right)^2$$

where D_{Na+} was the diffusion coefficient of Na^+ in working electrode. mB, VM, and MB were mass (g), molar volume ($cm^3\ mol^{-1}$), and relative molar weight of the cathode sample ($g\ mol^{-1}$), respectively. S was the surface area of the cathode (cm^2). τ was the applied current pulse time on the cathode (s). ΔE_S was the change of voltage during two consecutive steady states (V), and $\Delta E\tau$ was the voltage difference after a single pulse (V).

The diffusion coefficients Na^+ was calculated by fitting the CV curves at different scan rates by the Randles- Sevcik equation, as shown below:

$$D^{0.5} = \frac{1}{268700 \times A \times C \times n^{1.5}} \times \frac{I_p}{v^{0.5}}$$

Where I_p is the normalised peak current ($A\ mg^{-1}$), n is the number of electrons transferred during the redox reaction, A is the geometrical surface area of the electrode (cm^2), C is the molar concentration of sodium ions ($mol\ cm^{-3}$), v is the scanning rate ($V\ s^{-1}$), and D is the sodium ion diffusion coefficient ($cm^2\ s^{-1}$).

Theoretical calculation: All the calculations in this work were performed by using the Vienna Ab initio Simulation Package (VASP). The valence electron and core-ion interactions were described using the projected augmented wave (PAW). The electron exchange and correlation energies were calculated using the generalized gradient approximation/Perdew–Burke–Ernzerhof (GGA/PBE) exchange-correlation functional. The Brillouin zone was sampled by the Γ-centered k-mesh with a resolution

of $2\pi \times 0.04 Å^{-1}$ for geometry optimization and $2\pi \times 0.02 Å^{-1}$ for electronic structure calculation. The plane-wave energy cutoff was set to 500 eV, and the convergence tolerance for residual force and energy on each atom during structure relaxation were set to 0.02 eV/Å and 10^{-5} eV, respectively. The Hubbard U correction method was employed, with $U_{(Ni\ 3d)} = 6.2$ eV, $U_{(Fe\ 3d)} = 4.3$ eV, $U_{(Mn\ 3d)} = 3.9$ eV, $U_{(Ti\ 3d)} = 4.2$ eV as reported in previous studies. Van der Waals interaction (DFT-D3 method with Becke-Jonson damping) was incorporated. The VASPKIT code is used to finish the pre- and post-processing of the calculation results. The COHP calculations were carried out using local-orbital basis suite towards electronic structure reconstruction (LOBSTER) code.

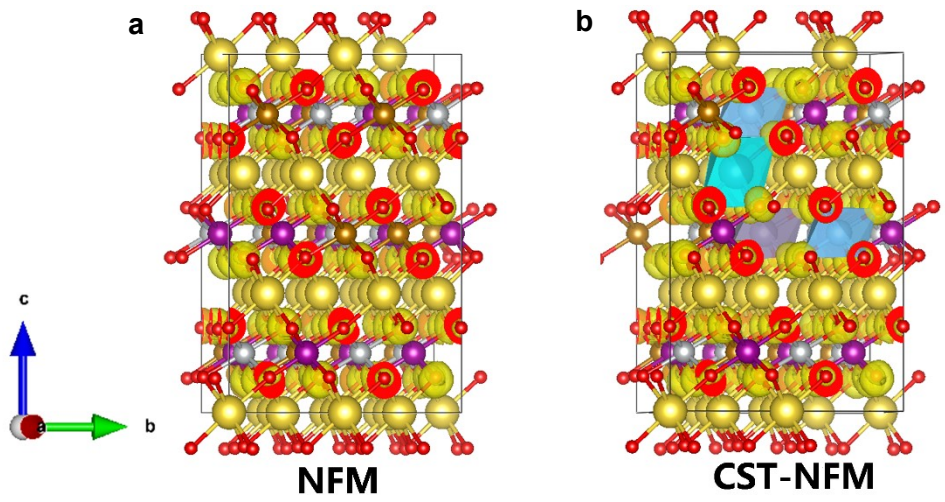

Figure S1. The electron density map of (a) NFM and (b) CST-NFM.

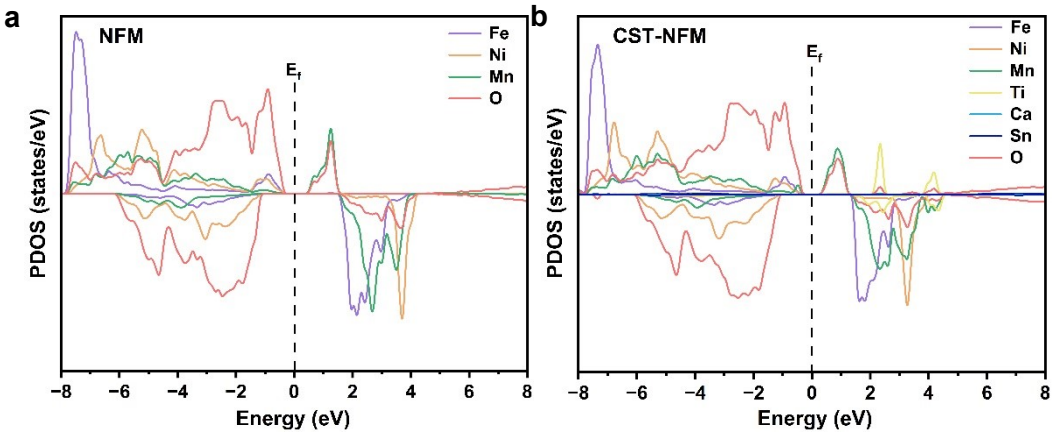

Figure S2. PDOS of (a) NFM and (b) CST-NFM.

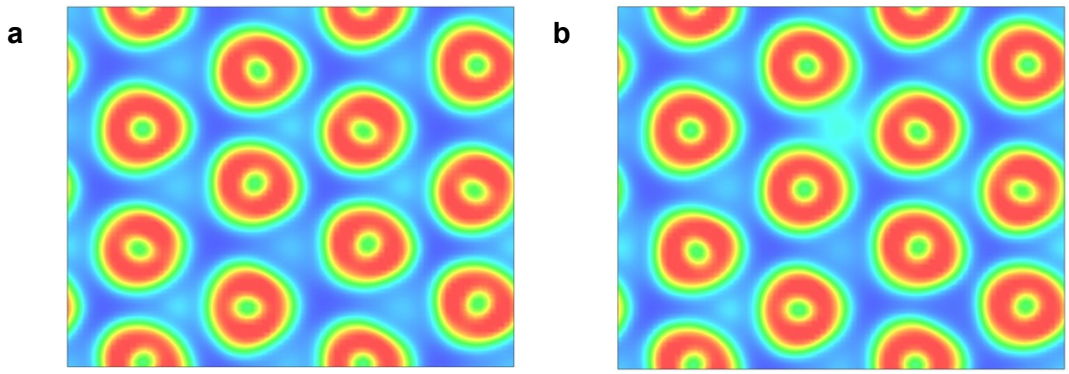

Figure S3. ELF of the valence electron in O-layer viewed along the [001] direction.

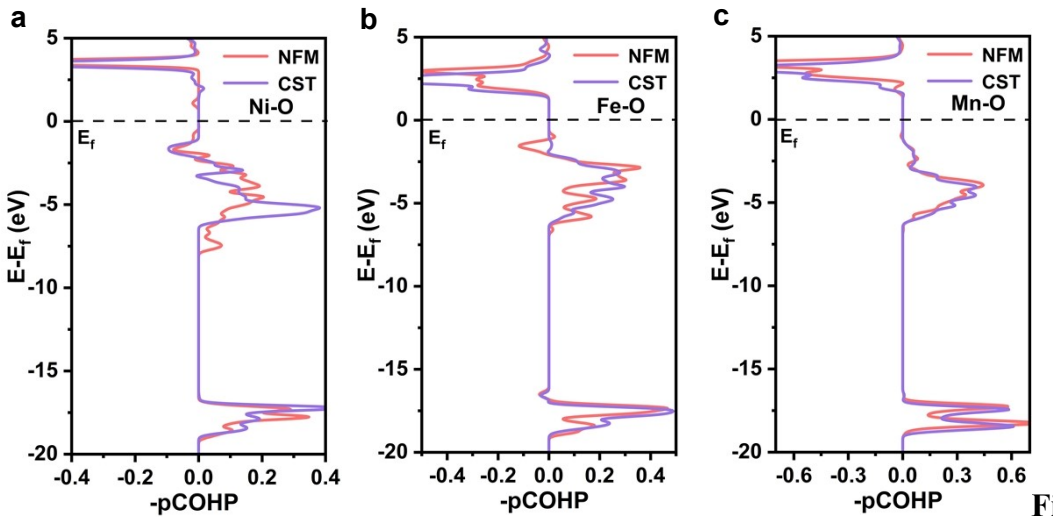

Figure S4. COHP results for NFM and CST-NFM on (a) Ni−O, (b) Mn−O, and (c) Fe−O bonds.

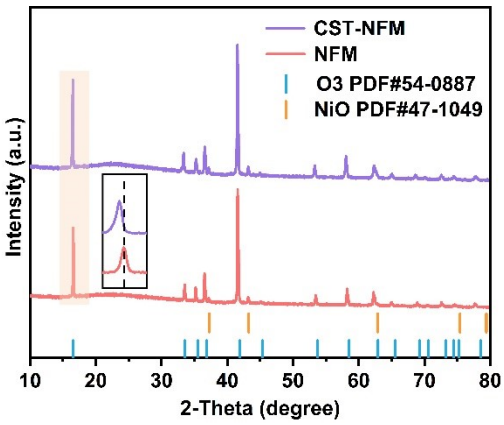

Figure S5. XRD patterns of NFM and CST-NFM.

1 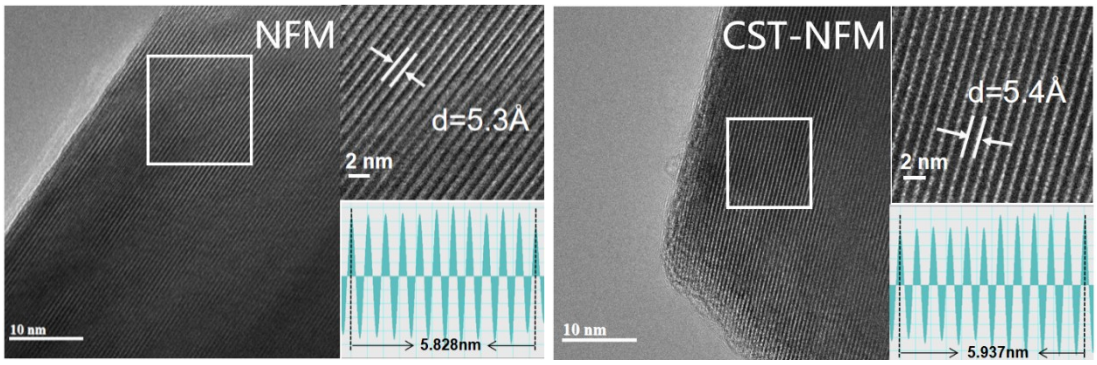

2 **Figure S6.** TEM images of NFM and CST-NFM.

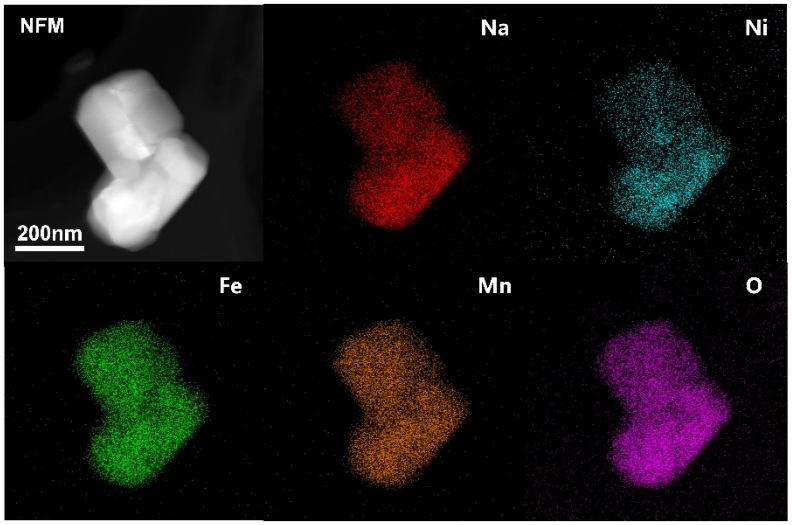

Figure S7. Elemental mappings of NFM.

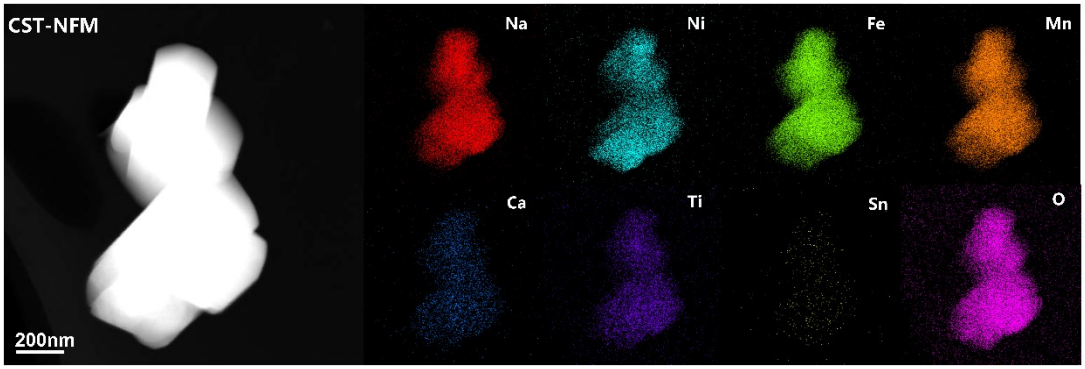

Figure S8. Elemental mappings of CST-NFM.

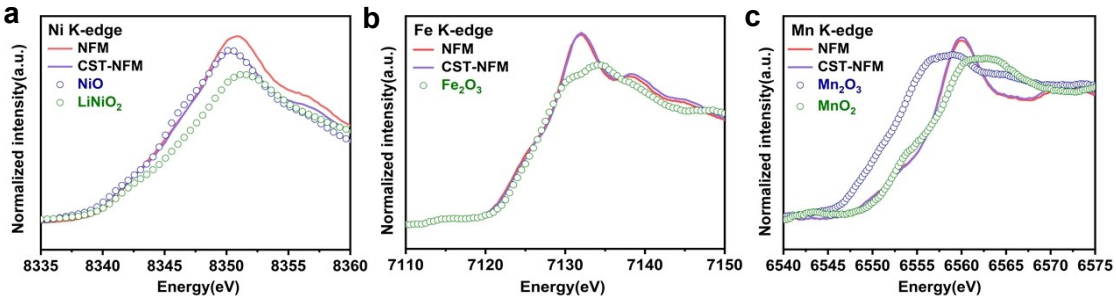

Figure S9. (a) Ni, (b) Fe and (c) Mn K-edge XANES spectra of NFM and CST-NFM.

1 

2 **Figure S10.** Atomic-scale EDS mapping of Ca in CST-NFM.

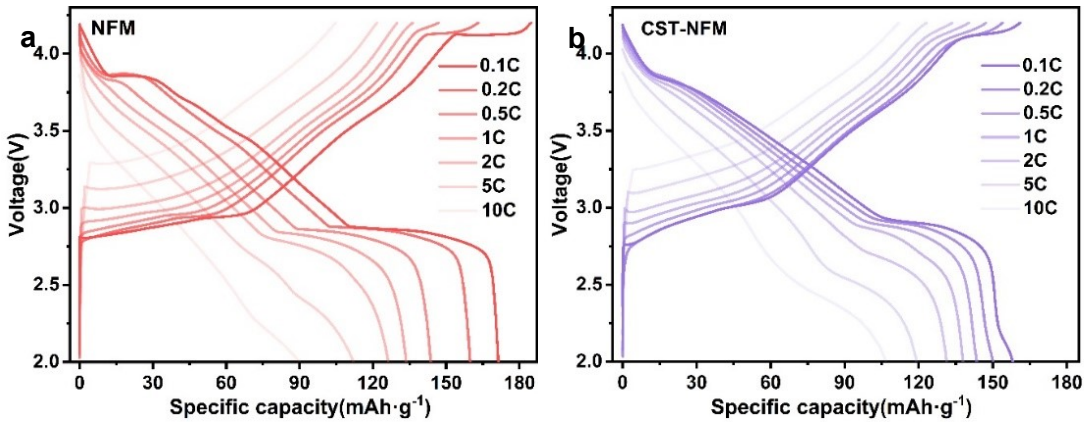

Figure S11. Charge/discharge curves of (a) NFM and (b) CST-NFM from 0.1 to 10 C.

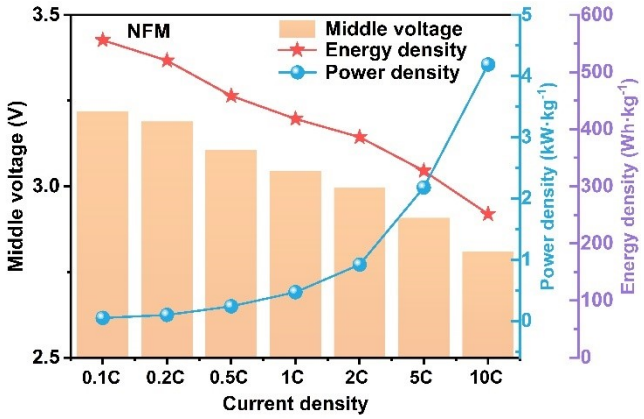

Figure S12. The middle voltage, energy density, and power density of NFM.

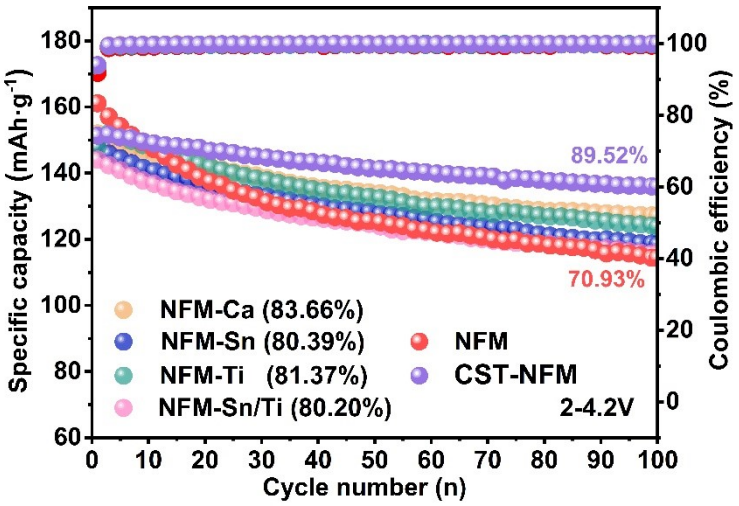

Figure S13. Cycling performance of the comparative samples at 1C.

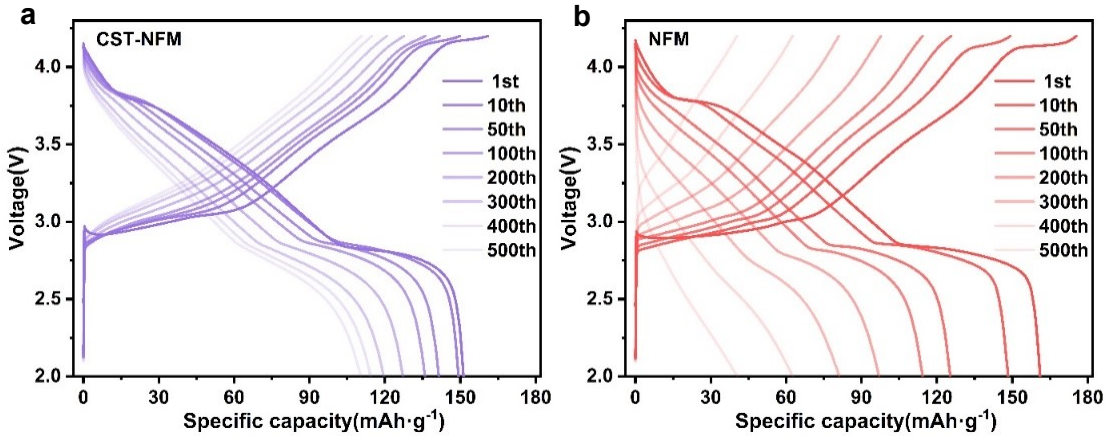

Figure S14. Charge/discharge profiles of (a) NFM and (b) CST-NFM at 1C.

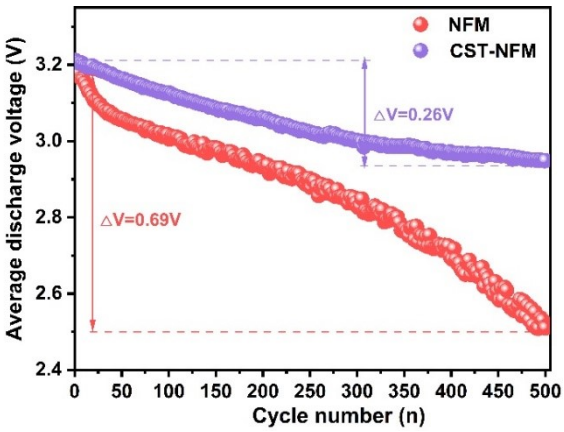

Figure S15. Average discharge voltage during the long-term cycling.

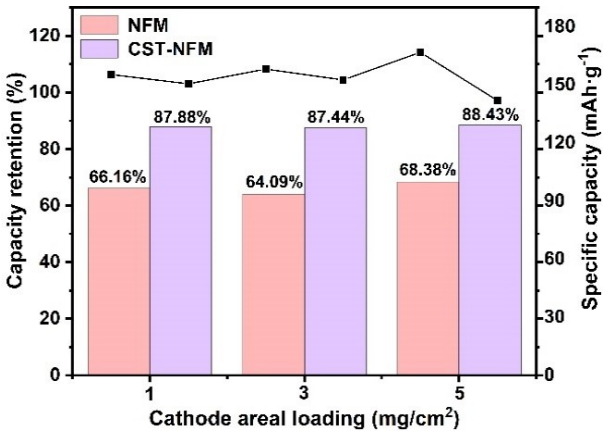

Figure S16. Cycling Performance of NFM and CST-NFM with different areal loadings.

1 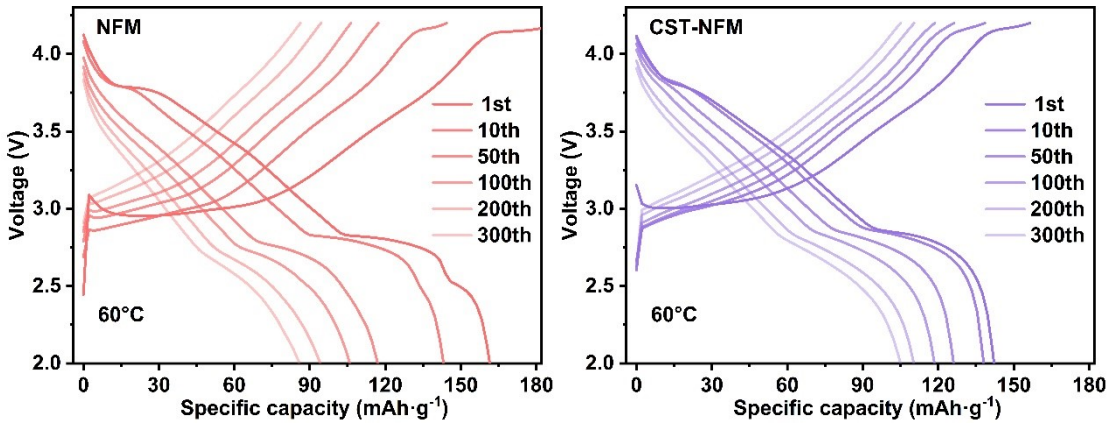

2 **Figure S17.** Charge/discharge profiles of (a) NFM and (b) CST-NFM at 60°C high
3 temperature.

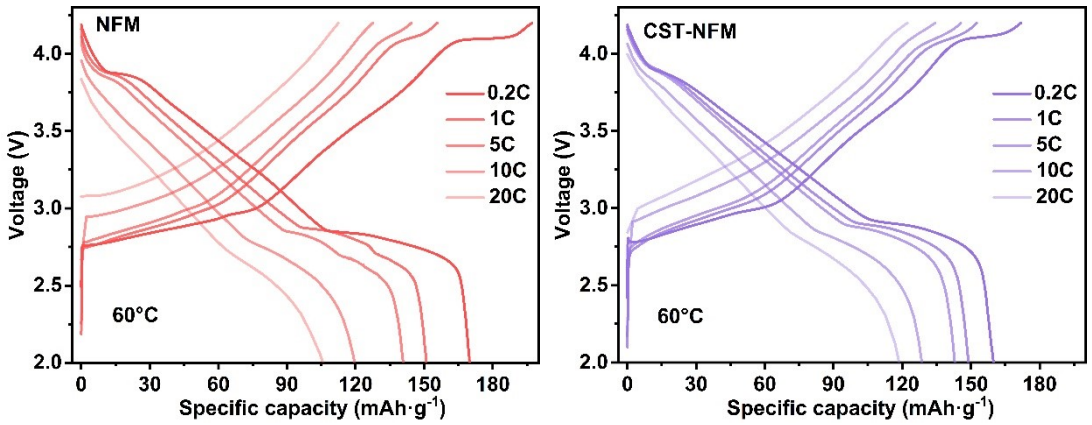

Figure S18. Charge/discharge curves of (a) NFM and (b) CST-NFM from 0.2 to 20 C at 60°C high temperature.

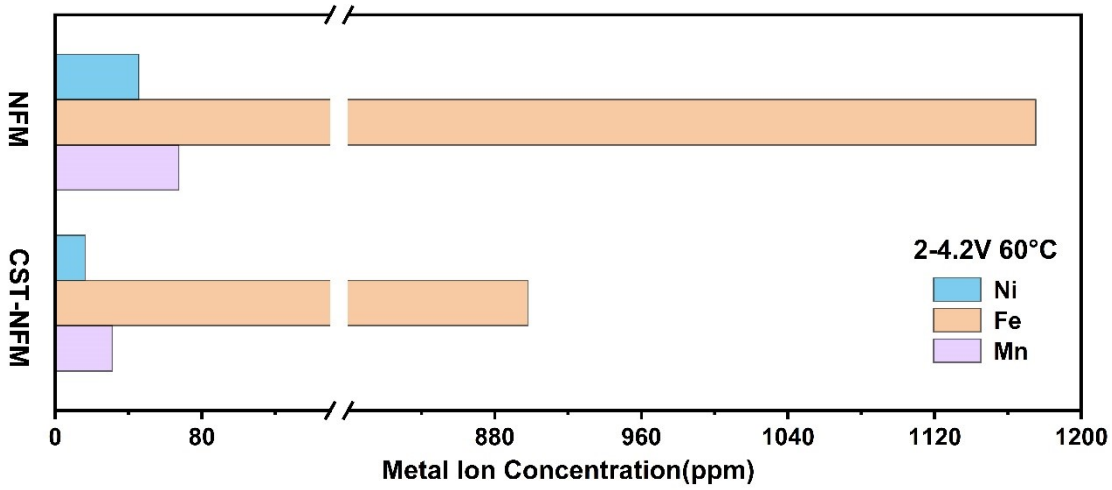

Figure S19. Concentrations of deposited transition metal ions in NFM||Na and CST-NFM||Na after 100 cycles at 60℃.

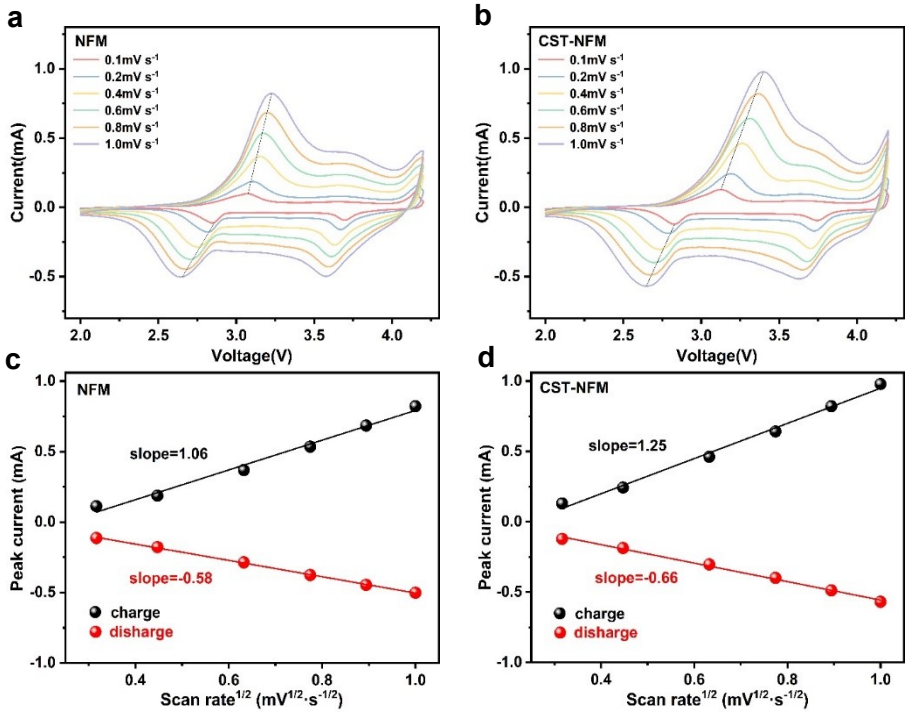

Figure S20. CV curves of (a) NFM and (b) CST-NFM at different scan rates. The plot of the peak current of (c) NFM and (d) CST-NFM as a function of the square root of scan rates.

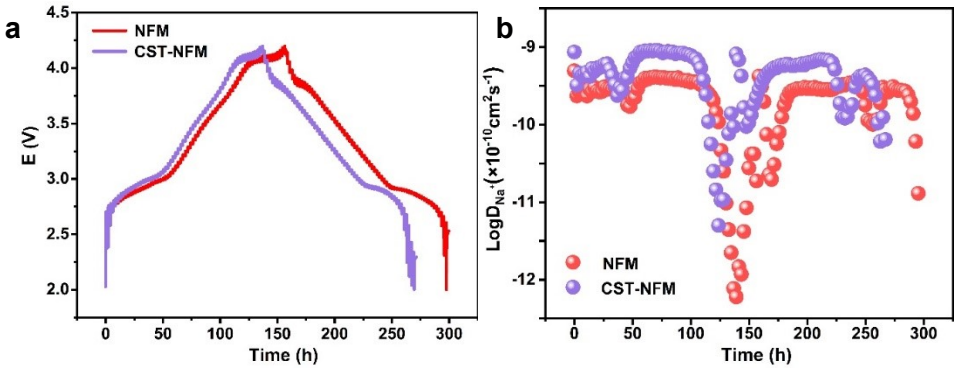

Figure S21. GITT curves of (a) NFM and (b) CST-NFM at 0.1C.

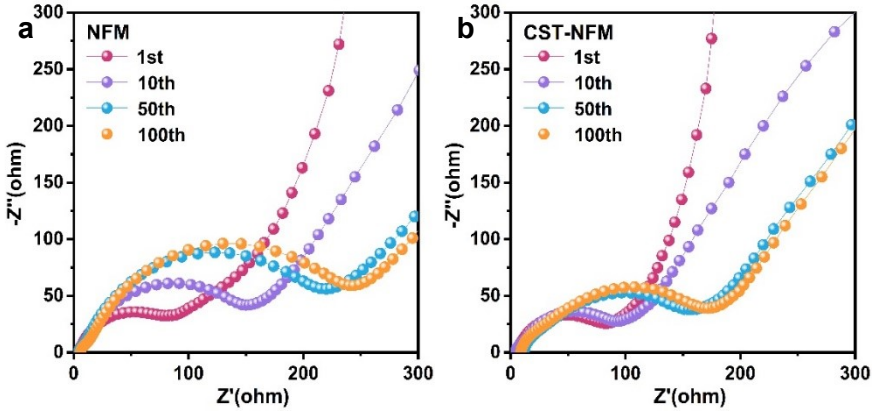

Figure S22. EIS results of (a) NFM and (b) CST-NFM after cycles.

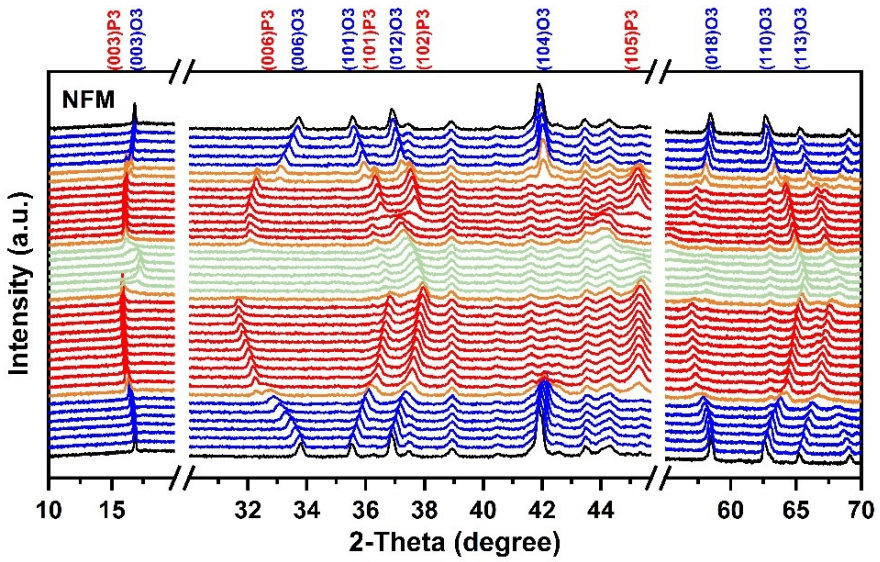

1

2 **Figure S23.** In-situ XRD patterns of NFM between 2.0 and 4.2 V at 30 mA g^{-1}.

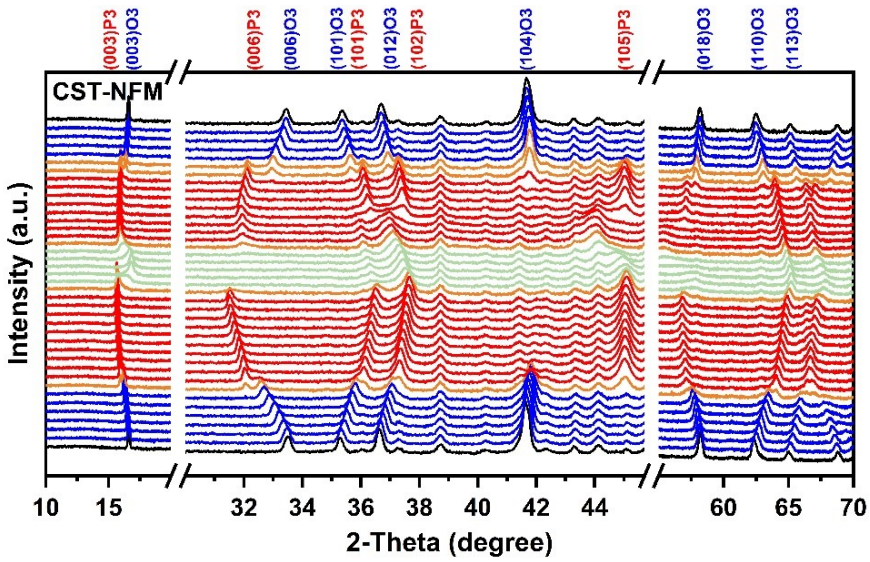

Figure S24. In-situ XRD patterns of CST-NFM between 2.0 and 4.2 V at 30 mA g^{-1}.

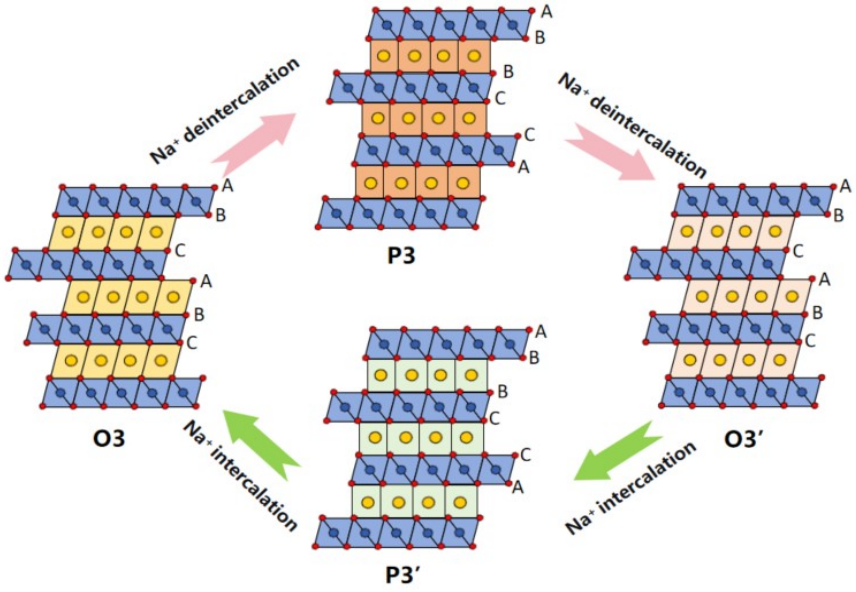

Figure S25. Schematic illustration of structural evolution of NFM and CST-NFM during charge/discharge process.

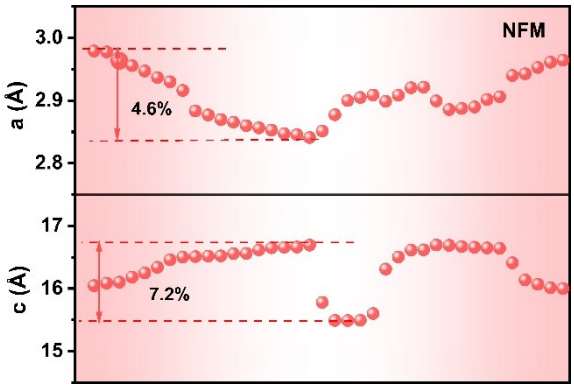

Figure S26. Variation of lattice constants of NFM.

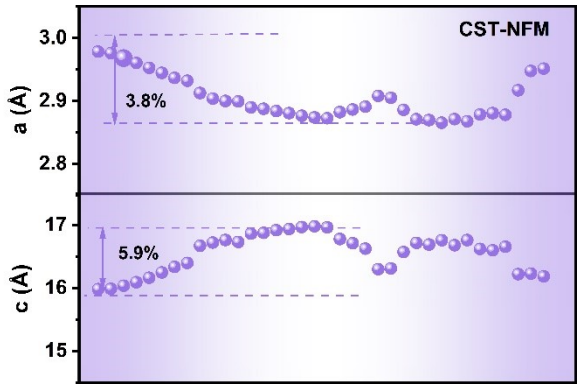

Figure S27. Variation of lattice constants of CST-NFM.

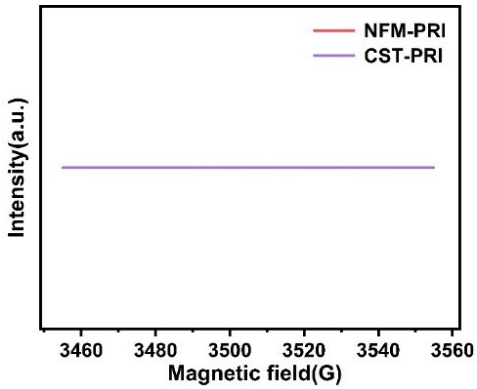

Figure S28. EPR results of NFM and CST-NFM at the initial state.

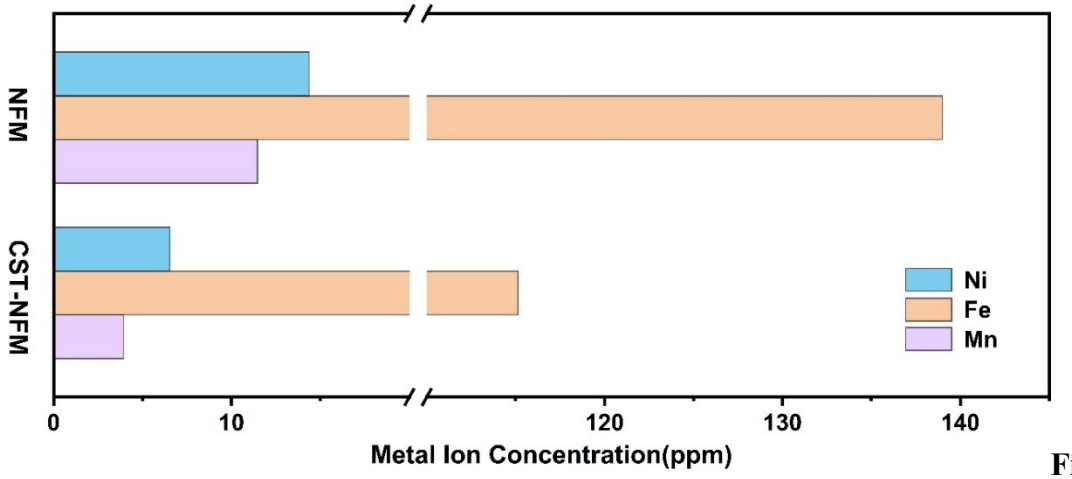

Figure S29. Concentrations of deposited transition metal ions in NFM||Na and CST-NFM||Na after 200 cycles.

1 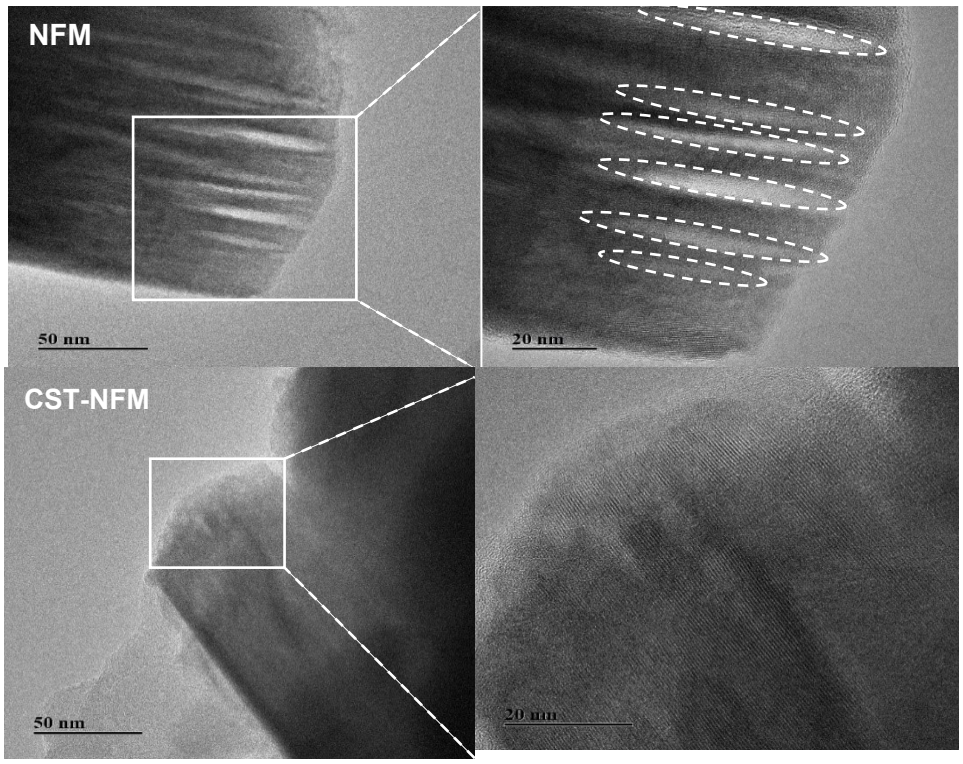

2 **Figure S30.** TEM images of NFM and CST-NFM after 200 cycles.

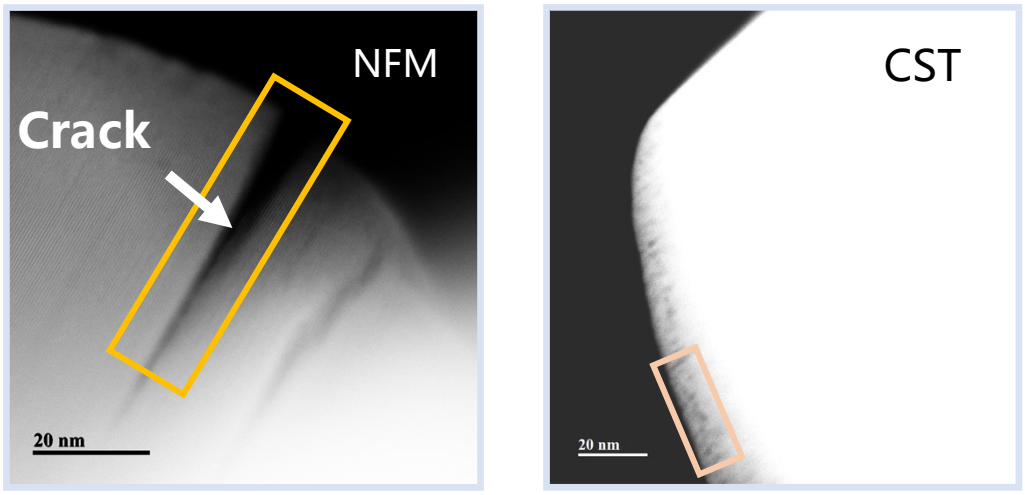

Figure S31. HAADF-STEM images of NFM and CST-NFM after 200 cycles.

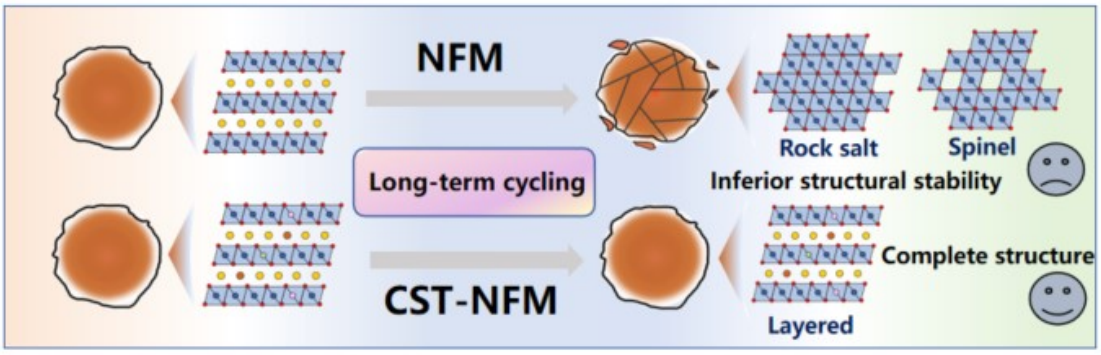

Figure S32. Schematic illustration of the structural degradation mechanism.

1

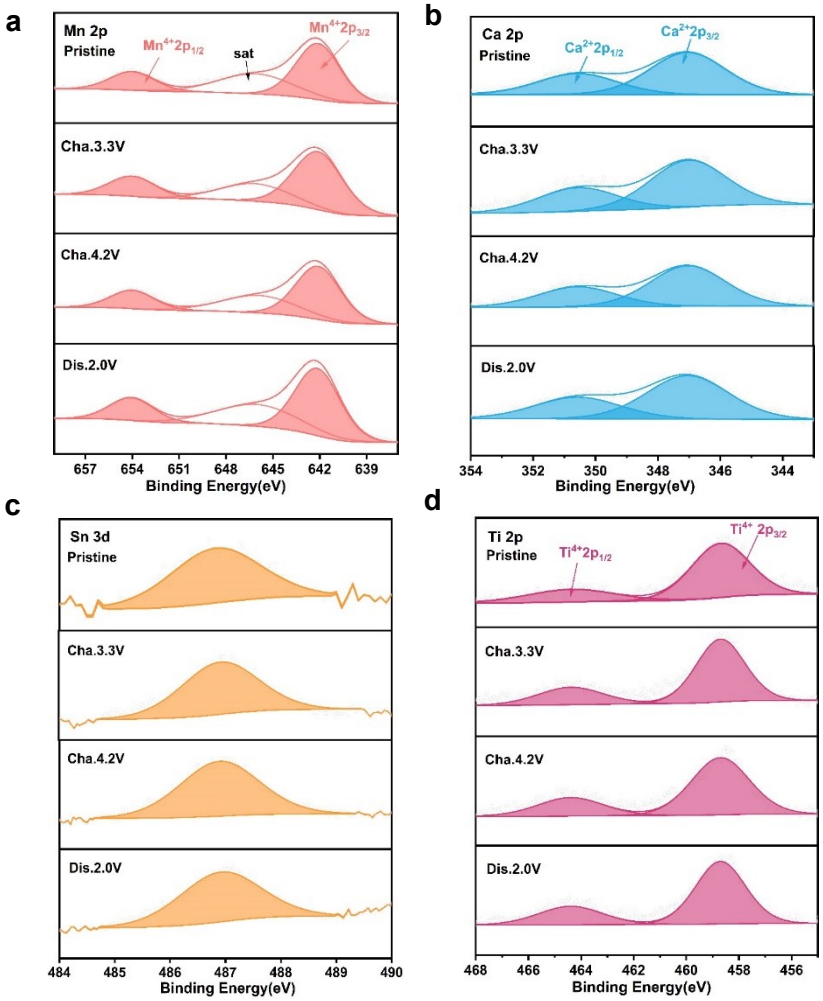

2

3 **Figure S33.** XPS spectra of (a) Mn 2p, (b) Ca 2p, (c) Sn 3d and (d) Ti 2p in CST-NFM
4 at various charge/discharge states.

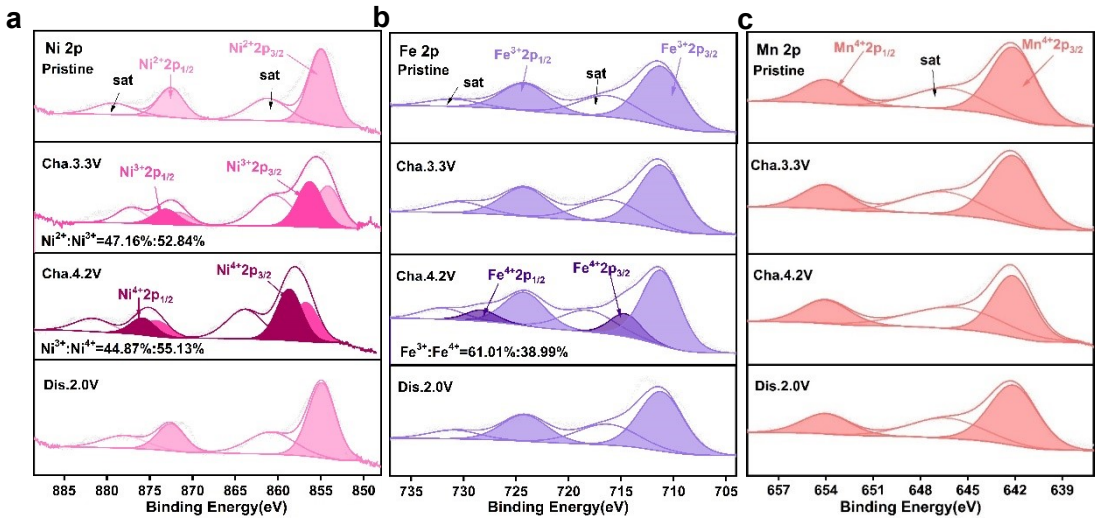

Figure S34. XPS spectra of (a) Ni 2p, (b) Fe 2p and (c) Mn 2p in NFM at various charge/discharge states.

1 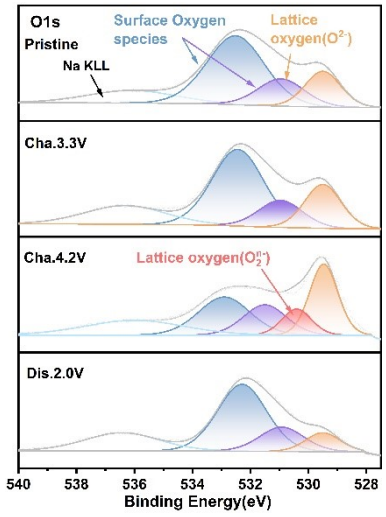

2 **Figure S35.** XPS spectra of O 1s in NFM at various charge/discharge states.

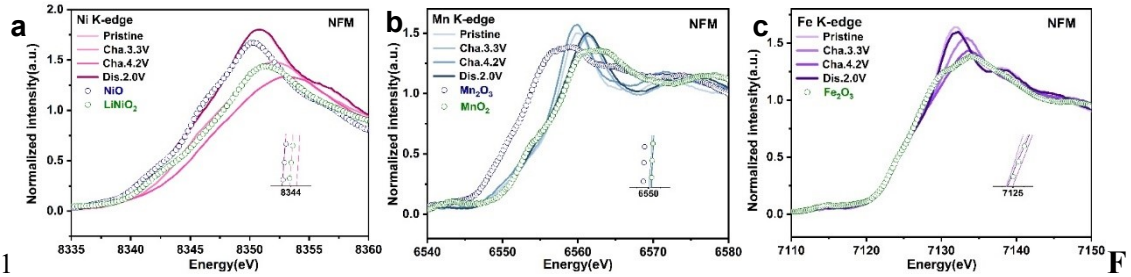

Figure S36. (a) Ni, (b) Fe and (c) Mn K-edge XANES spectra of NFM at different charge/ discharge states.

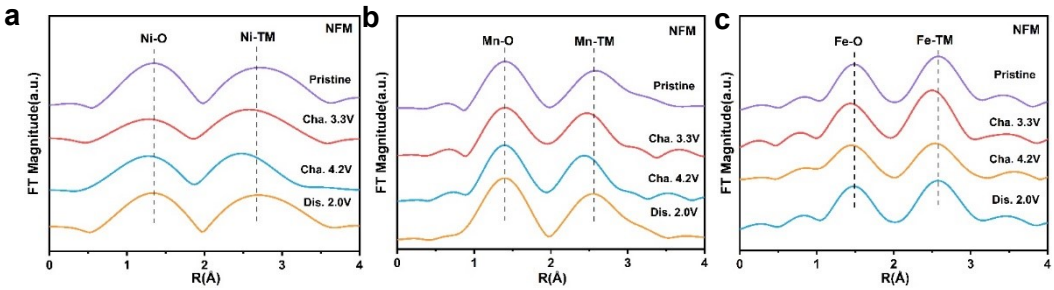

Figure S37. (a) Ni, (b) Fe and (c) Mn K-edge FT-EXAFS spectra of NFM at different charge/discharge states.

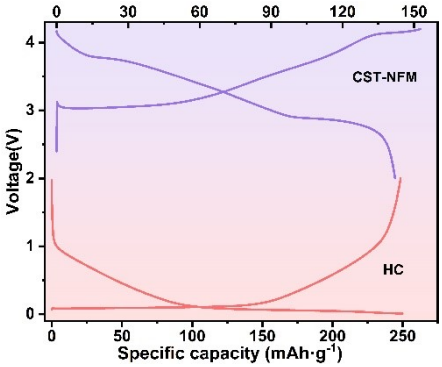

Figure S38. Initial galvanostatic charge/discharge curves of HEO cathode and HC anode after precycled.

1 **Table S1**. ICP-OES and ISE results of NFM and CST-NFM.

Theoretical chemical composition	Composition from ICP						
Materials	Na	Ca	Ni	Fe	Mn	Ti	Sn
$NaNi_{0.33}Fe_{0.33}Mn_{0.33}O_2$	1.000	N/A	0.325	0.328	0.336	N/A	N/A
$Na_{0.98}Ca_{0.01}Ni_{0.33}Fe_{0.28}Mn_{0.315}Ti_{0.05}Sn_{0.015}O_2$	0.980	0.011	0.369	0.295	0.320	0.056	0.016

2

Table S2. XRD refinement results of NFM and CST-NFM.

Parameter	a (Å)	b (Å)	c (Å)	V (Å^3)	$d_{(O\text{-}TM\text{-}O)}$ (Å)	$d_{(O\text{-}Na\text{-}O)}$ (Å)
NFM	2.9802	2.9802	16.0366	123.3490	2.3492	2.9964
CST-NFM	2.9770	2.9770	16.1242	123.7570	2.2610	3.1140

Table S3. Crystallographic and Rietveld refinement data of NFM.

NFM (R-3m)		R_{wp}=5.15 %, R_p = 2.61%			
Atom	Site	x	y	z	Occ
Na	3a	0	0	0.000	1.023
Ni	3b	0	0	0.500	1.021
Fe	3b	0	0	0.500	
Mn	3b	0	0	0.500	
O	6c	0	0	0.240	1.008

Table S4. Crystallographic and Rietveld refinement data of CST-NFM.

CST-NFM (R-3m)		R_{wp}=5.49%, R_p =3.20%			
Atom	Site	x	y	z	Occ
Na	3a	0	0	0.000	0.957
Ca	3a	0	0	0.000	
Ni	3b	0	0	0.500	0.971
Fe	3b	0	0	0.500	
Mn	3b	0	0	0.500	
Sn	3b	0	0	0.500	
Ti	3b	0	0	0.500	
O	6c	0	0	0.237	0.952